Disordered mesoporous polymer derived N-doped TiO2/Si-O-C-N nanocomposites with nanoscaled heterojunctions towards enhanced adsorption and harnessing of visible light

Eranezhuth Wasan Awin, Abhijeet Lale, K.C. Hari Kumar, Samuel Bernard, Ravi Kumar

Disordered mesoporous polymer derived N-doped TiO_2/Si-O-C-N nanocomposites with nanoscaled heterojunctions towards enhanced adsorption and harnessing of visible light

Eranezhuth Wasan Awin[a], Abhijeet Lale[b], K.C. Hari Kumar[a], Samuel Bernard[b], Ravi Kumar[a,]

[a] Laboratory for High Performance Ceramics, Department of Metallurgical and Materials Engineering, Indian Institute of Technology-Madras (IIT Madras), Chennai 600036, India
[b] Univ. Limoges, CNRS, IRCER, UMR 7315, F-87000 Limoges, France

Keywords:
Mesoporous
Nanocomposite
Photocatalysis

Adsorption
Heterojunction

ABSTRACT

The mesoporous N-doped TiO_2/Si-O-C-N ceramic nanocomposites has been revealed to be a potential candidate towards visible light photocatalytic degradation of organic dyes. The polymer-derived ceramic route was implemented to prepare uniformly distributed in-situ crystallized N-doped TiO_2 nanocrystals in a mesoporous amorphous siliconoxycarbonitride matrix. This chemical approach assisted by the hard template pathway resulted in a high surface area (186 m^2/g) nanocomposite exhibiting predominantly mesoporous structure with an average pore size of 11 nm. The two-step process involved pyrolysis of the polyhydridomethyilsiloxane impregnated in CMK3 (hard template) under argon generating SiOC-C composites and functionalizing it with titanium n-tetrabutoxide to be pyrolyzed under ammonia to form the titled nanocomposite. Interestingly, pyrolysis in a reactive ammonia atmosphere resulted in the incorporation of nitrogen in the titania lattice while decomposing the template. The Si-O-C-N support on which N-doped TiO_2 exhibited superior adsorption of organic dye molecules and photocatalytically active in the visible wavelength. The nanoscaled heterojunctions reduced the recombination rate and the presence of superoxide anions/hydroxyl radicals was found to be responsible for the dye degradation.

1. Introduction

Titania (TiO_2), known for its photocatalytic applications ever since its discovery by Fujishima and Honda [1] has attracted a lot of interest in the research community ranging its application from hydrogen pro-duction and water purification to solar cells [2–5]. The low cost, oxi-dizing power and durability of TiO_2 has made it a material of interest. However, the band gap of TiO_2 of 3.2 eV restricts itself from harnessing of light in the visible wavelength thereby limiting its photocatalytic activity in the UV region [6]. Several methods have been explored to-wards the reduction of band gap of TiO_2 which includes doping of TiO_2 with non-metals such as C, N, F, P and S [7–10]. The introduction of dopants generates an impurity state above the valence band of TiO_2, hence raising the valence band edge, resulting in the absorption of visible light. Ever since Asahi et al. reported the reduction of band gap in nitrogen-doped TiO_2 (N-TiO_2) and improved absorption of solar light [11], various approaches have been adopted towards synthesis of N-doped TiO_2 photocatalysts. This includes sol-gel reaction [12], solvothermal reaction [13,14] and hydrothermal reaction [15]. Re-cently, titanium oxynitride (Ti-O-N) microspheres were synthesized by ammonolysis of TiO_2 microspheres and were reported to exhibit visible light photocatalytic activity [15]. Visible light photocatalytic activity of mesoporous N-TiO_2 possessing high surface area was also reported to absorb light in the visible light regime [15].

The retrieval of dispersed photocatalysts from aqueous solution as well as the agglomeration of TiO_2 nanoparticles hinders the im-plementation of the material for water purification applications. Anchoring/immobilizing the photocatalysts on a suitable substrate is an alternative way to overcome the above mentioned disadvantage. TiO_2 immobilized on high surface area mesoporous SBA-15 was shown to act as an active photocatalyst [16]. The mesoporous substrate with high surface area plays a prominent role in determining the adsorption characteristics, thereby influencing the overall reaction rate. Precursor routes such as the Polymer-Derived Ceramics (PDCs) approach enable controlling the size, composition, porosity and shape of the final pro-duct [17–19]. The amorphous Si-O-C-N possess enhanced properties

Corresponding author.
E-mail address: nvrk@iitm.ac.in (R. Kumar).

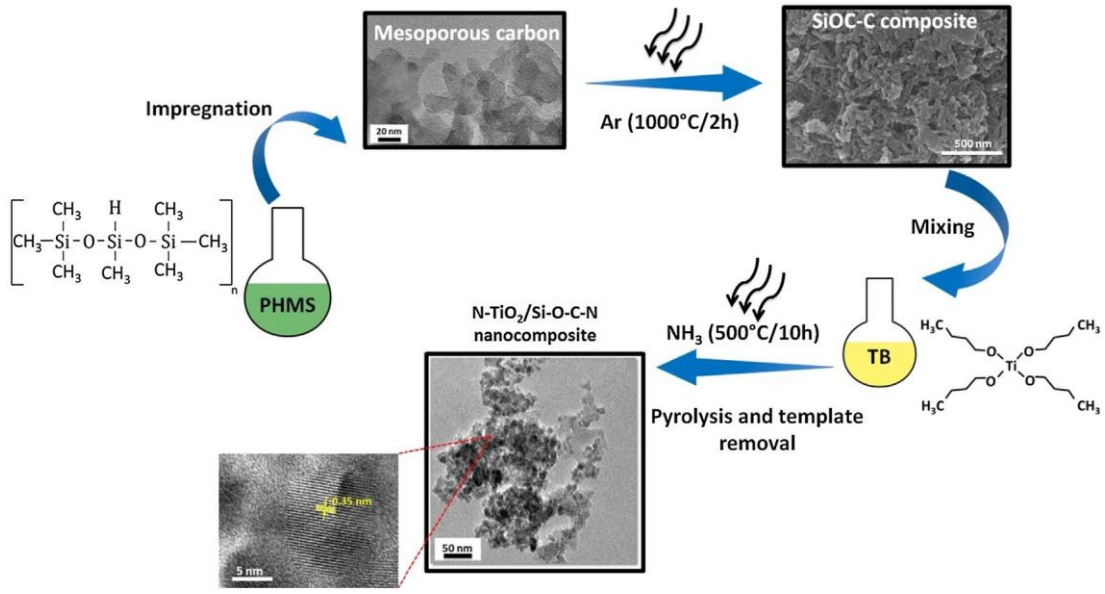

Fig. 1. Schematic representing the generalized processing route for the synthesis of the mesoporous nanocomposite.

such as thermal stability, creep resistance, chemical stability and oxi-dation resistance [20–22]. Hence, Si-O-C-N ceramics in the form of composites, fibers, coatings and membranes offers to be a potential candidate in extreme/harsh operating conditions. For instance, ex-cellent adsorption capacity was shown by hierarchically porous silicon-carbon-nitrogen (Si-C-N) ceramics prepared from preceramic polymers in contrast to its bulk counterparts [23]. Such materials were shown to be highly efficient in removing organic pollutants. The template as-sisted PDCs approach results in porous structures with high stability, surface area and tailorable pore size [24]. In the current study, a two-step template assisted PDCs approach has been adopted to synthesize uniformly distributed N-doped TiO_2 anchored on an amorphous Si-O-C-N matrix possessing high surface area and disordered mesoporous structure, especially by tailoring the chemistry of precursors and using their reactivity with ammonia as a reactive atmosphere. The resulting material was evaluated for its photocatalytic activity towards de-gradation of methylene blue in visible light.

2. Experimental section

2.1. Synthesis of the mesoporous nanocomposite

0.2 g of mesoporous carbon (Sigma-Aldrich, Bangalore, India) was kept at 100 °C overnight to remove the moisture present in the pores. Subsequently 1 ml of polyhydridomethyilsiloxane (PHMS, Sigma-Aldrich, Bangalore, India) was impregnated into mesoporous carbon by stirring the mixture in vacuum for 24 h. The mixture was then trans-ferred to an alumina crucible and pyrolyzed at 1000 °C in argon at-mosphere at a heating rate of 2 °C/min and held for 2 h. The pyrolyzed product, SiOC-C composite was then mixed with 1 ml of titanium n-tetrabutoxide (TB, Sigma-Aldrich, Bangalore, India) stirred overnight and subsequently pyrolyzed in ammonia atmosphere at 500 °C for 10 h maintaining a heating rate of 5 °C/min.

2.2. Characterization

The powder X-ray diffraction (XRD, D8 Discover, Bruker AXS X-ray diffractometer, USA) was carried out to understand the phase evolution. The Raman spectrum (Labram HR800, Horiba, Japan) was recorded in the range of 100 and 2000 cm^{-1} using a He-Ne laser source. The sur-face morphology as well as the size distribution of the particles was studied in assistance with scanning electron microscopy (SEM, Hitachi S-4800, Japan) and transmission electron microscopy (TEM, JEOL 3010, Japan). The sample was sputter coated for 80 s prior to SEM analysis so as to avoid the charging effects. To perform the TEM ana-lysis, the sample was dissolved in acetone, ultrasonicated for 15 min and a couple of drops were poured on the copper grid. In order to quantify the porosity, the sample was degassed at 150 °C for 6 h and adsorption–desorption isotherm was obtained at −196 °C using BET analyzer (TriStar 3020, Micromeritics, USA). The pore size distribution was determined using Barrett–Joyner–Halenda (BJH) method. The XPS measurements (Omnicron nanotechnology, ESCA-14, Germany) were carried out using Al K_α (1486.6 eV) as radiation source. The deconvo-lution of the spectra was done using CASA XPS software. The calibra-tion of the spectra was done with respect to C1s peak at a binding energy value of 284.8 eV. The bonding characteristics were studied with the aid of FTIR spectroscopy (Perkin Elmer Spectrum, USA). The solid state ^{29}Si NMR was recorded using Bruker AV III, Germany spectrometer operating at 500 MHz.

2.3. Photocatalytic studies

To evaluate the photocatalytic activity of the nanocomposite, me-thylene blue (0.06 and 0.12 mM) was chosen as the representative dye and 50 mg of the catalyst was added to 100 ml of the solution. The mixed solution was then kept for 12 h in dark to achieve ad-sorption–desorption equilibrium. Subsequently, the solution was stirred and subjected to visible light exposure (500 W tungsten halogen lamp). At regular time intervals, 2 ml of the solution was taken out and cen-trifuged, to remove the catalyst. The concentration of the MB was measured using UV–vis spectrophotometer (ThermoFisher Scientific, Evolution 220, USA).

3. Results and discussion

PHMS, with a chemical structure of $(CH_3)_3SiO[(CH_3)HSiO]_nSi(CH_3)_3$ was used as the molecular precursor for the synthesis of silicon oxycarbide (SiOC) matrix. The pyrolysis of PHMS in an inert atmo-sphere leads to amorphous SiOC. Herein, PHMS was infiltrated into CMK3 to replicate the nanostructured mesoporous structure by nano-casting. The functionalization of the composite with titanium was done using TB ($Ti(OCH_2CH_2CH_2CH_3)_4$) and the template was reduced by pyrolyzing in a reactive ammonia atmosphere. The overall reaction procedure is shown in Fig. 1.

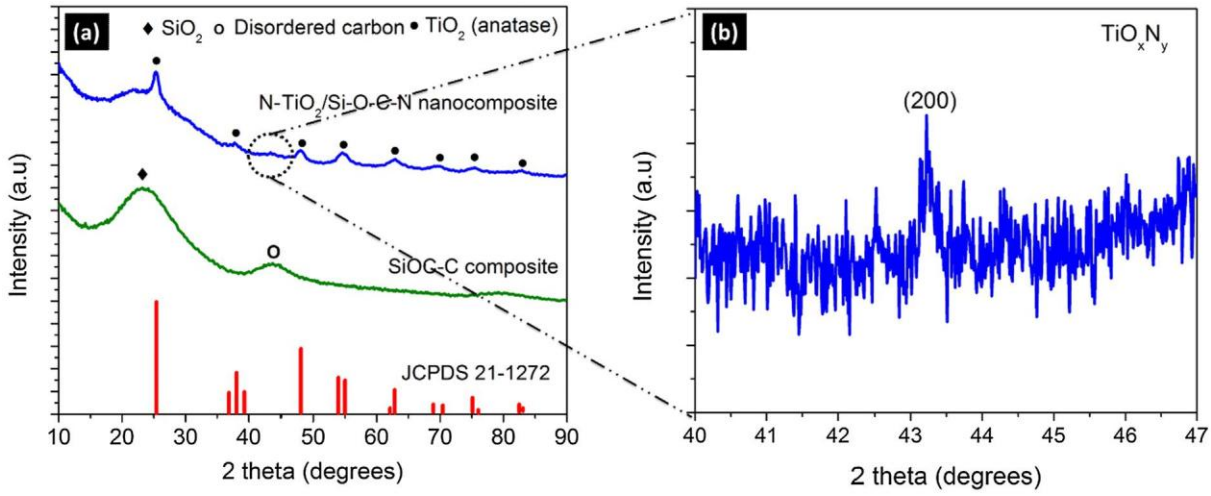

Fig. 2. (a) X-ray diffractograms revealing the amorphous and crystalline phases of the nanocomposite before and after functionalization with TB and (b) The slow scan XRD of N-TiO_2/Si-O-C-N exemplifing the TiO_xN_y phase.

The XRD pattern of SiOC-C composite before functionalization with TB was characteristic of an amorphous compound with broad peaks at 2θ ~ 23° and 43.8°. The broad hump at 23° corresponds to either amorphous SiO_2 [25] or the presence of SiOC [26]. The peak at 2θ ~ 43.8° corresponds to the characteristic amorphous disordered carbons [27]. The XRD of N-TiO_2/Si-O-C-N nanocomposite (after functionalization with TB and ammonia treatment) clearly reveals the crystallization of anatase phase with major peaks at 2θ = 25.3°, 37.8° and 48.0° corresponding to (1 0 1), (0 0 4) and (2 0 0) planes of anatase, respectively (Fig. 2a). Interestingly, an additional peak was observed at 2θ ~ 43° and has been assigned to the (2 0 0) plane of titanium oxy-nitride (TiO_xN_y) phase (Fig. 2b). The initiation of the crystallization of TiO_xN_y phase is an indication of gradual transformation of anatase phase with prolonged holding hours in ammonia atmosphere. The Scherrer equation was used to calculate the crystallite size of anatase and was found to have an average size of 5 nm.

The analysis of Raman spectra (Fig. 3) indicated the presence of six bands at 151 cm^{-1} (E_g), 201 cm^{-1} (E_g), 399 cm^{-1} (B_{1g}), 505 cm^{-1} (A_{1g}), 519 cm^{-1} (B_{1g}) and 630 cm^{-1} (E_g) confirming the presence of anatase phase. This is in good agreement with the XRD result. The inset image shows the presence of D and G peaks at 1348 cm^{-1} and 1588 cm^{-1} respectively attributing to the existence of free carbon. The

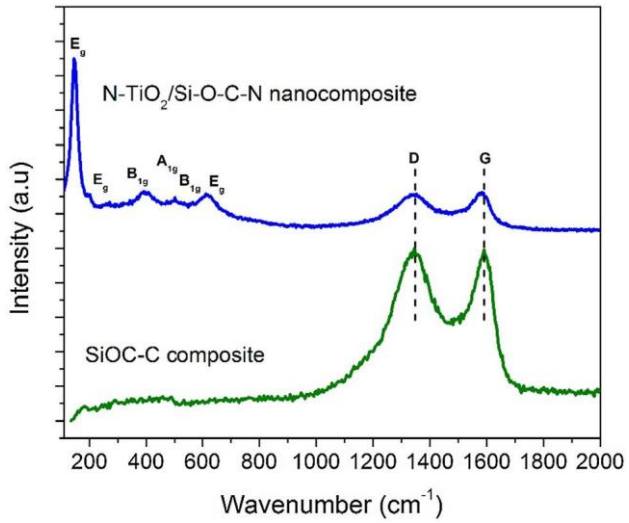

Fig. 3. Raman spectra of the nanocomposite before and after functionalization with TB implying the presence of anatase phase and free carbon.

pyrolysis in reactive atmosphere such as ammonia is known to reduce the carbon entities via. transamination reactions during the initial stages of polymer to ceramic conversion [28,29]. However, the high affinity of titanium atoms towards nitrogen could hinder this reaction. This could result in the formation of free carbon by the phase separation of SiOC at higher temperatures. The Raman spectra of SiOC-C compo-site (i.e., before functionalization with TB) clearly revealed the for-mation of free carbon as a result of the phase separation of SiOC. Nevertheless, the carbon template is believed to be reduced because of its decomposition under ammonia.

The scanning electron micrographs of mesoporous carbon (CMK-3) and the TiO_xN_y-derived materials are shown in Fig. 4a and b respec-tively. This clearly indicates that the structure of the hard template is indeed retained in the nanocomposite after nitridation process which highlight Raman discussion on the identification of carbon in our ma-terials. This also displays the fact that the polymer impregnated well in to the pores of the carbon template. The EDS spectrum of the nano-composite is shown in Fig. 4c. The EDS spectra clearly reveals the presence of silicon, oxygen, carbon, titanium and nitrogen.

The structural organization of the sample was analyzed using transmission electron microscopy (TEM). The micrograph clearly re-veals the presence of well-defined crystals that are uniformly dis-tributed on a support matrix (Fig. 5a). At higher magnification, the lattice fringe interplanar spacing of 0.35 nm represents the (1 0 1) plane of anatase (Fig. 5b). The crystals exhibit a spherical morphology with an average crystal size of 5–10 nm, which substantiated the XRD re-sults.

The nitrogen adsorption-desorption isotherm exhibit a typical type IV curve with a H2 hysteresis loop revealing the mesoporous nature of the nanocomposite as exemplified in Fig. 6. The impregnation/pyrolysis process resulted in the reduction of BET surface area from 478 m^2/g for CMK-3 to 186 m^2/g for the nanocomposite. The Barrett-Joyner-Halenda (BJH) pore size distribution profile is presented as an inset image and the mean pore size was found to be 11 nm. The pore volume was found to be 0.29 cm^3/g. The surface area, pore volume and pore size of SiOC-C composite was revealed to be 350 m^2/g, 0.45 cm^3/g and 19 nm re-spectively. The decrease in pore volume and surface area of the me-soporous SiOC-C composite after functionalization with TB then an-nealing under ammonia confirms SEM observation and most probably the presence of the TiO_2 phase as nanocrystals identified by TEM in the porous structure of the pristine SiOC-C composite.

The incorporation of nitrogen in the material was confirmed by XPS as observed in Fig. 7. The deconvolution of N1s peak (Fig. 7b) resulted in three peaks at 397.2, 399.4 and 402.2 eV. The peak at 397.2 eV could

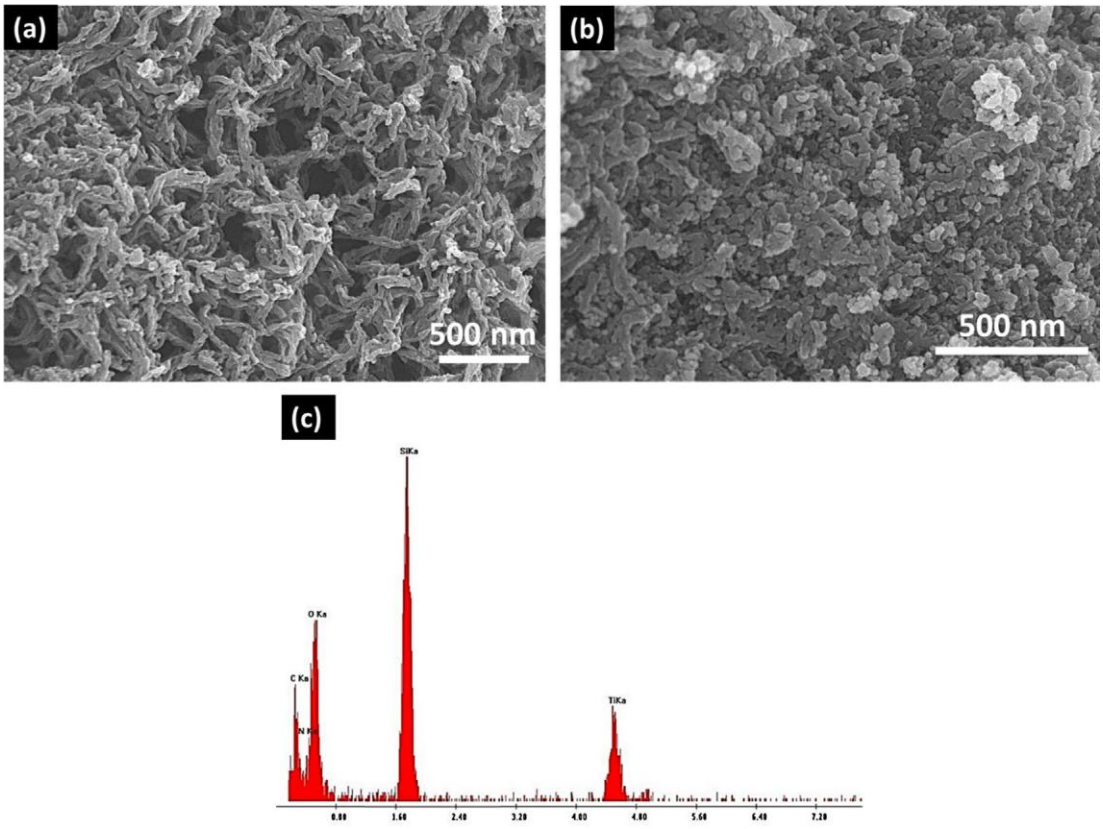

Fig. 4. Scanning electron micrograph exhibiting the porous nature of (a) CMK-3 (b) the TiO_xN_y-derived materials and (c) EDS spectrum of the nanocomposite.

be assigned to the NeTieN bonds implying the nitrogen ions occupying the substitutional sites and is close enough to the reported values of TiN [11,30]. The peak at 399.4 eV corresponds to the TieNeO and TieOeN linkage which could be ascribed to the positively charged N^+ ions lo-cated at the interstitial site of TiO_2 lattice [31]. The substitution of N_2 in OeTieO structure results in reduced electron density around N and increase in binding energy of N1s peak in OeTieN environment in contrast to that of NeTieN. Reports suggest that both substitutional and interstitial type N evokes visible light photocatalytic activity. The presence of signal at 402 eV could be attributed to the NH_3 chemi-sorbed or molecular N_2 onto TiO_2 [31].

The XPS spectra of Ti 2p spectra resulted in peaks at binding en-ergies of 459.8 eV and 465.5 eV corresponding to Ti $2p_{3/2}$ and Ti $2p_{1/2}$ respectively (Fig. 7a). The diff erence in binding energy of 5.7 eV be-tween the doublets confirmed that titanium exists in Ti 4+ oxidation state. This indicates that there is negligible amount of transfer of electron from oxygen vacancies to titanium atoms [32]. The Si $2p_{1/2}$ peak (Fig. 7d) exhibited a signal at binding energy 103.5 eV indicating the presence of SiO_4 units on the surface of the nanocomposite [33]. Fig. 7c shows the C1s spectra of the mesoporous nanocomposite. The main peak at 284.8 eV corresponds to CeC and the three peaks at 285.8, 287.5 and 289.4 eV corresponds to C]N, CeN and CeO bonds

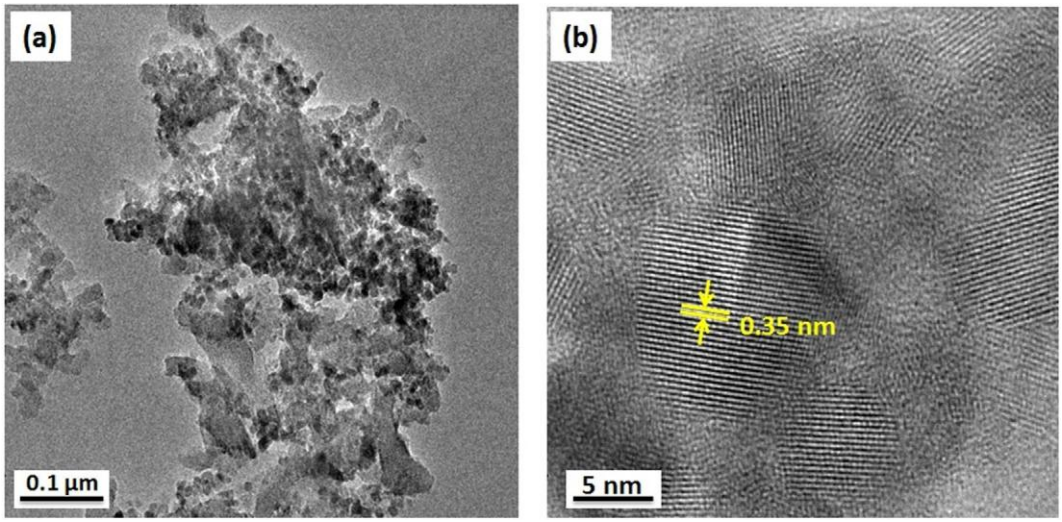

Fig. 5. Transmission electron micrograph illustrating (a) uniform distribution of the TiO_xN_y-derived materials and (b) Lattice fringes unveiling a spacing of 0.35 nm consigned to (1 0 1) plane of the anatase phase in the TiO_xN_y-derived materials.

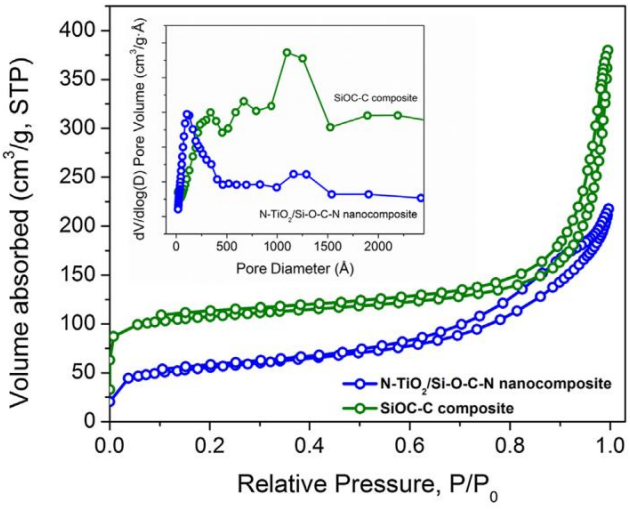

Fig. 6. N_2 adsorption-desorption isotherm indicating the presence of mesopores in SiOC-C composite and N-TiO_2/Si-O-C-N nanocomposite and the inset image shows the BJH pore size distribution curve.

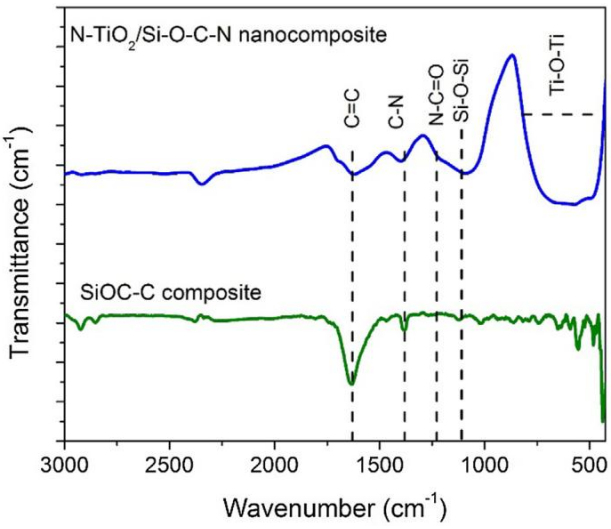

Fig. 8. FTIR spectrum showing the bonding characteristics of the SiOC-C composite and N-TiO_2/Si-O-C-N nanocomposite.

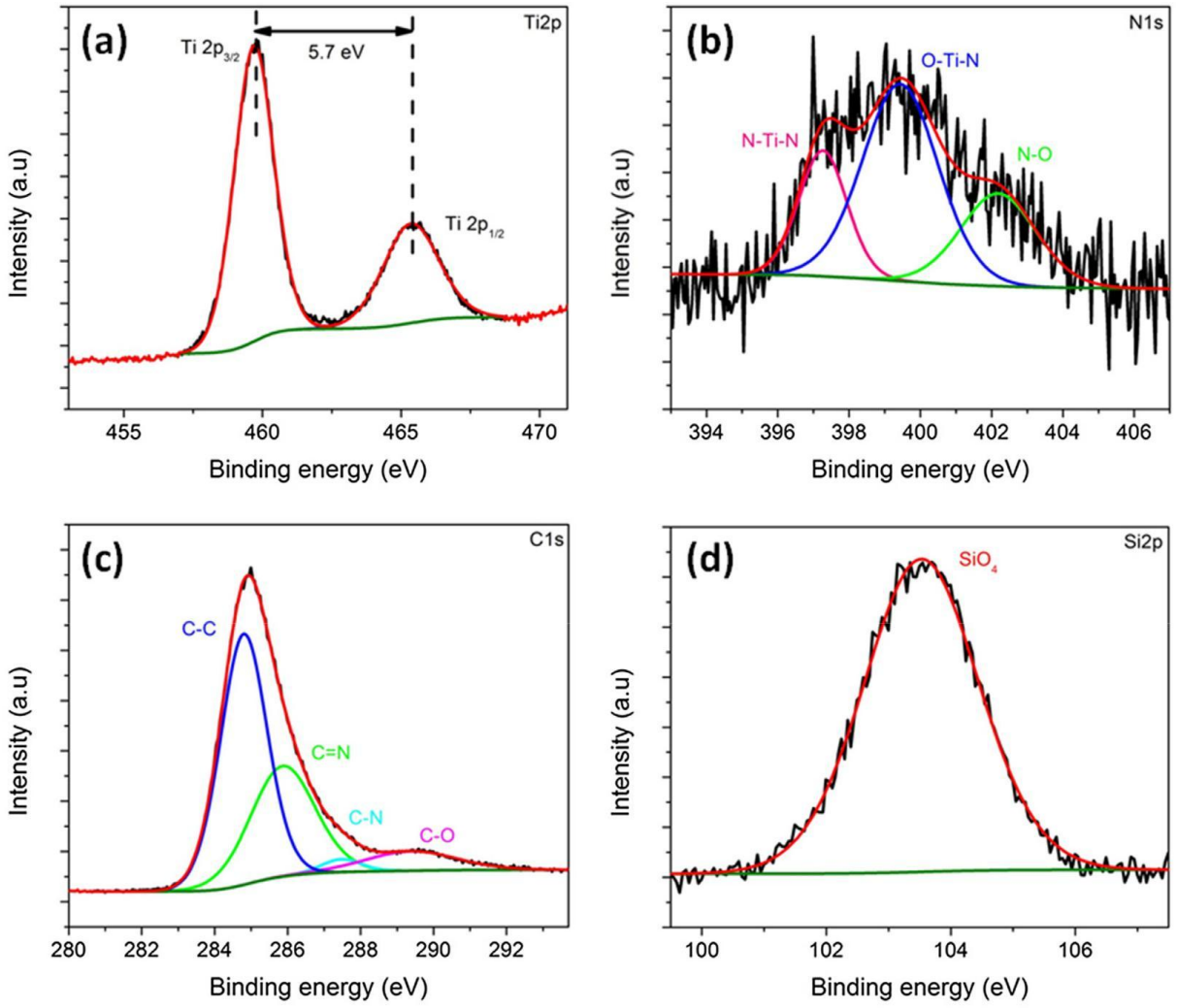

Fig. 7. XPS spectra (a) Ti2p (b) N1s (c) C1s and (d) Si2p of the nanocomposite.

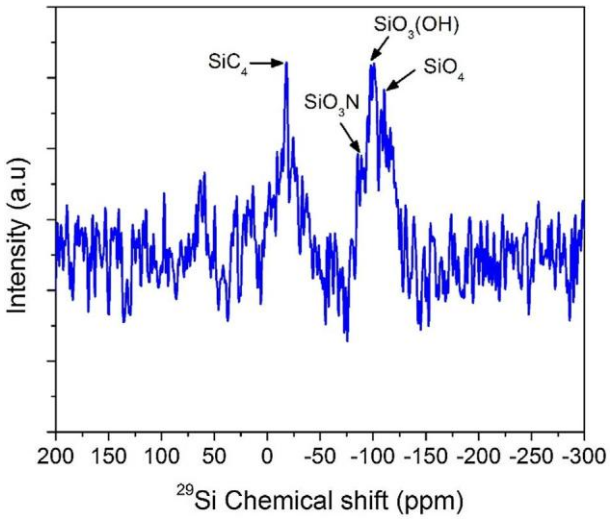

Fig. 9. ^{29}Si MAS NMR spectra of N-TiO_2/Si-O-C-N nanocomposite implying the incorporation of N atoms in the Si-based network.

respectively [34,35]. This in turn suggests that the amorphous matrix to be composed of CeNeO bonds.

XPS clearly highlights the presence of a TiO_xN_y most probably supported by a SieOeC matrix. FTIR of the SiOCeC composite and mesoporous nanocomposite were also performed to understand the chemical bonding and is exemplified in Fig. 8. The FTIR spectrum of SiOCeC composite shows a peak at 1630 cm^{-1} corresponding to C]C bond [23], indicating the presence of mesoporous carbon. In the case of mesoporous nanocomposite, the broad peak at around 1000–1100 cm^{-1} and 600–800 cm^{-1} corresponds to the presence of SieOeSi bonds and TieOeTi stretching modes respectively [36]. The peak at around 1420 cm^{-1} corresponds to the CeN bond [34]. This further confirms the incorporation of nitrogen into the amorphous matrix. Apart from this, the peak at 1210 cm^{-1} corresponding to NeC]O was also observed [37]. Hence, it is understood that pyr-olyzing in ammonia atmosphere not only leads to the doping of ni-trogen into TiO_2 lattice but also modifies the amorphous matrix.

The local environment around silicon atoms was further in-vestigated by analyzing the NMR spectrum shown in Fig. 9. The peaks present at −100 ppm and −109 ppm could be attributed to SiO_3(OH) and SiO_4 units, respectively. The shoulder peak at −90 ppm could be assigned to SiO_3N units, where Si atoms share bonds with oxygen and nitrogen atoms [38,39]. The occurrence of SiO_3N peak implies the fact that the pyrolysis of the molecular precursor under ammonia atmo-sphere has led to the incorporation of nitrogen atoms in the Si-based network. The signal at −18 ppm corresponds to SiC_4. In general, be-sides the presence of SiC_4 and SiO_4 signals, the silicon oxycarbide based ceramics exhibits additional resonance peaks at SiO_3C (−70 ppm), SiO_2C_2 (−35 ppm) and $SiOC_3$ (6 ppm) [40]. The absence of these mixed bonds implies that the ammonolyzed sample has undergone phase se-paration at higher temperatures resulting in the formation of multi-phasic system and free carbon. The XRD and Raman spectra (Figs. 2 and 3) also substantiate the aforementioned fact.

Fig. 10a shows the absorption spectra of MB solution of 0.06 mM kept in dark for 12 h. It is clearly observed that due to the ultra-high adsorption capacity exhibited by the nanocomposite, most of the MB molecules gets adsorbed on to the material system which results in complete decolourization of the solution. Hence, in order to compre-hend the kinetics of photocatalytic degradation in visible light, the concentration of MB solution was doubled to 0.12 mM. The absorption spectrum of MB solution (0.12 mM) before and after exposure of visible light is exemplified in Fig. 10b. As seen from the spectrum, the con-centration of the MB solution gradually decreases with increase in irradiation time indicating the reaction of catalyst with the solution in the presence of light. The photocatalytic activity of the nanocomposite in visible light could be ascribed to the doping of nitrogen in the TiO_2 lattice.

In order to determine the photodegradation constant, Langmuir – Hinshelwood kinetic model was used which determines the photo-catalytic activity independent of the amount of MB concentration left in the solution [41]. The experimental data was fitted using first order kinetic equation, $\ln(C/C_o) = -kt$ where C is the concentration of the MB at time t, C_o is the initial concentration and k is the photo-degradation constant. The plot of ln C/C_o vs time follows a first order reaction in which ln C/C_o linearly decreases with time as depicted in Fig. 10c. The photocatalytic degradation constant, k($\times 10^{-3}$ min^{-1}) was calculated to be 8.3. The UV–vis diffuse reflectance spectrum of the N-TiO_2/SiOCN nanocomposite exhibited a very strong absorption in the visible to near infra-red region as shown in Fig. 10d. However, no specific band edge was observed in the UV-DRS spectrum. This could be due to the presence of amorphous Si-O-C-N matrix present in the na-nocomposite, since the Bloch theorem is no longer applicable in amorphous materials due to the lack of lattice periodicity, leaving the crystalline hk momentum unidentified [42].

The BET surface area of the N-TiO_2/SiOCN nanocomposite was found to be 130 m^2/g after the adsorption/catalysis experiments (Fig. 11) in contrast to 186 m^2/g for the nanocomposite before the experiments. This further proves the fact that pores play a major role in the adsorption process.

In order to investigate the active species involved in dye degrada-tion, reaction species trapping experiments were carried out (Fig. 12). The isopropanol (0.02 M), benzoquinone (0.001 M) and triethanola-mine (0.01 M) were used as sacrificial agents for scavenging hydroxyl radicals ($^{\bullet}OH$), superoxide anion radicals ($^{\bullet}O_2^-$) and photogenerated holes (h^+) respectively. Fig. 12 shows the degradation efficiency of methylene blue with and without the presence of scavengers. It could be clearly understood that the methylene blue without the presence of catalyst showed highest degradation efficiency. The introduction of isopropanol drastically reduced the degradation efficiency, implying that $^{\bullet}OH$ plays a significant role towards the degradation of methylene blue dye. A decrease in degradation efficiency was also observed with the addition of triethanolamine, indicating that h^+ also has a minor role to play in the degradation process. However, the catalyst in the presence of benzoquinone had the least effect on the degradation effi-ciency, manifesting that $^{\bullet}O_2^-$ has minimal role to play in the catalytic degradation process.

The plausible mechanism for the visible light photocatalytic activity of N-TiO_2/Si-O-C-N nanocomposite is shown in Fig. 13a. The crystalline form of anatase transfers the electron from the valence band to the conduction band up on irradiation of an UV light, thereby favoring the photocatalytic reaction. However, since the band gap of TiO_2 being high, the electrons fails to excite in the visible light regime. The in-corporation of nitrogen in the TiO_2 lattice, substantiated by the XPS analysis, is believed to alter the electronic band structure of TiO_2. The doping of nitrogen atoms results in the creation of an additional N2p band above the O2p band, which results in the reduction of bang gap. Thus, instead of electron being excited from the O2p band (in pure TiO_2), diffusion of charge carriers occurs from the N2p band to Ti3d conduction band. The resulting electrons in the conduction band reduce with the oxygen molecules to produce superoxide ions, O_2^-. Con-comitantly, the holes in the valence band react with the water mole-cules to produce the hydroxyl radical, $OH^{\bullet}$. The aforementioned su-peroxide anions and the hydroxyl radical are believed to be responsible for the degradation of MB molecules. The heterojunction formation between amorphous Si-O-C-N and crystalline N-TiO_2 is expected to reduce the recombination rate as evident from HR-TEM micrograph (Fig. 13b). The heterojunction formation between the crystalline N-TiO_2 and amorphous Si-O-C-N matrix results in the migration of pho-togenerated electrons from the conduction band of amorphous Si-O-C-N

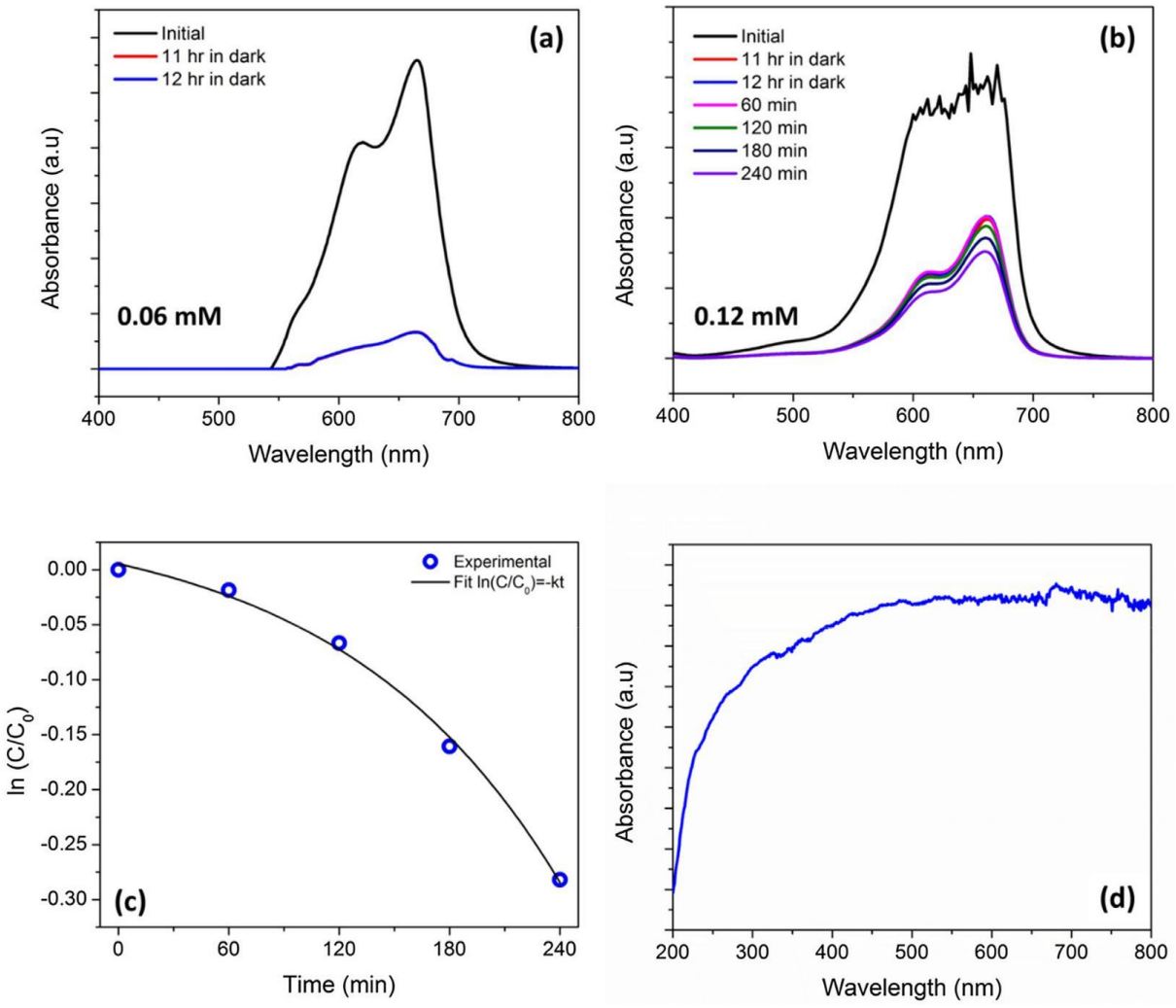

Fig. 10. UV–vis absorption spectra of (a) 0.06 mM of MB with 50 mg of the catalyst kept in dark for 12 h (b) 0.12 mM of MB with 50 mg of the catalyst exposed to visible light after keeping it in dark for 12 h (c) photocatalytic activity of the mesoporous nanocomposite and (d) UV-visible absorption spectrum of the mesoporous nanocomposite.

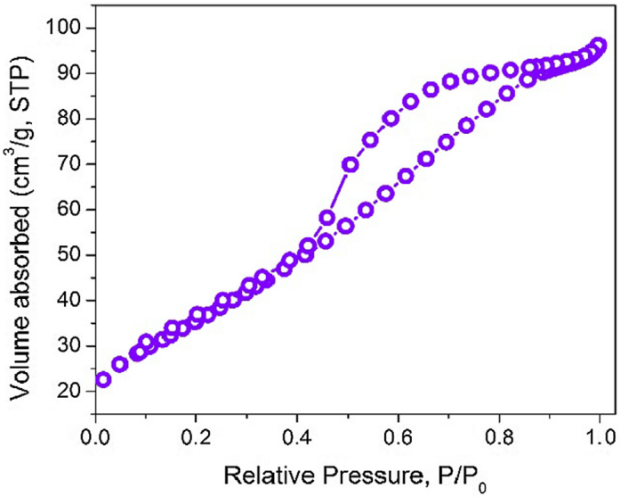

Fig. 11. . N_2 adsorption-desorption isotherm of the nanocomposite after the adsorption/catalysis.

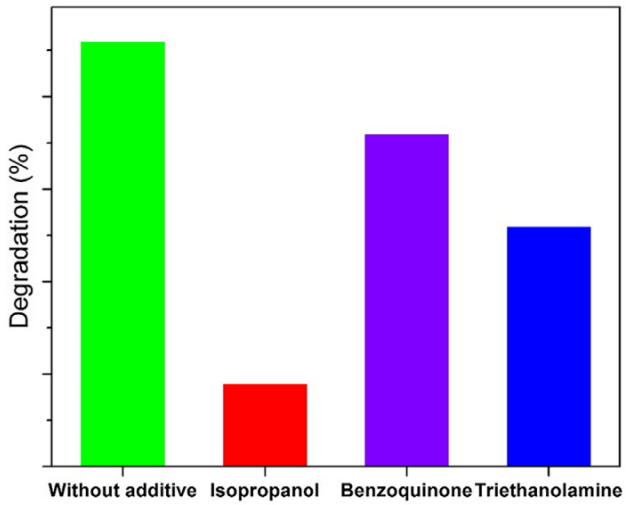

Fig. 12. . Catalytic degradation efficiency of methylene blue solution with and without the presence of presence of scavengers.

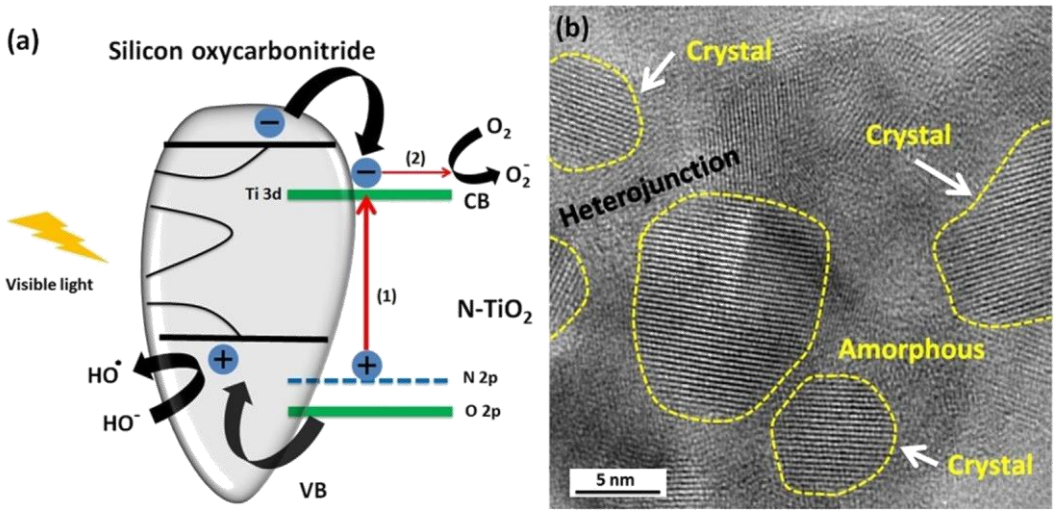

Fig. 13. (a) Schematic representing the visible light photocatalytic activity of the nanocomposite and (b) TEM micrograph exemplifying the heterojunction for-mation.

to the conduction band of N-TiO_2. Similarly, the photogenerated holes will migrate from the valence band of N-TiO_2 to the valence band of amorphous Si-O-C-N.

The reactions occurring during dye degradation could be general-ized as follows:

The methylene blue molecules gets adsorbed on to the surface which turns out to be the first step (Eq. (1)) in the catalytic process. Up on exposure to visible light, the charges are excited (Eq. (2)) to form $^{\%}O_2^-$ and $^{\%}$OH radicals.

N-TiO2/Si-O-C-N + Methylene blue Methylene blue-adsorbed N-TiO2/ Si-O-C-N (1)

Methylene blue -adsorbed N-TiO_2 + hν Methylene blue-adsorbed N-TiO_2 (e^-, h^+) (2)

However, as the reaction trapping experiments suggests, the $^{\%}$OH radicals are the major contributing species when compared to $^{\%}O_2^-$, indicating that $^{\%}O_2^-$ are unstable in aqueous solution resulting in im-mediate conversion to $^{\%}$OH radicals. The plausible degradation me-chanism is explained in the below mentioned reactions.

The $^{\%}O_2^-$ radicals are formed when photogenerated electrons reacts with the oxygen molecules as shown in Eq. (3) H_2O_2 are formed when $^{\%}O_2^-$ radicals gets disproportionated or reduced by an electron (Eq. (4)) and the formed H_2O_2 subsequently reacts with electrons to from $^{\%}$OH radicals as expressed in Eq. (5).

$$O_2 + e^- \rightarrow {}^{\%}O_2^-$$

$$^{\%}O_2^- + e^- + 2H^+ \rightarrow H_2O_2$$

$$H_2O_2 + e^- \rightarrow {}^{\%}OH + OH^-$$

The h^+ also reacts with the water molecules resulting in the for-mation of $^{\%}$OH radicals Eqs. (6) and (7).

$$H_2O \rightarrow H^+ + OH^- \quad 7)$$

$$OH^- + h^+ \rightarrow {}^{\%}OH$$

Finally, the $^{\%}$OH and $^{\%}O_2^-$ reacts with the dye methylene blue molecules decomposing into water, carbon dioxide (CO_2) and other inorganic compounds (Eqns. (8) and (9)).

$^{\%}$OH + dye → water + CO_2 + inorganic compounds $^{\%}O_2^-$

+ dye → water + CO_2 + inorganic compounds

4. Conclusions

A hard template assisted precursor derived approach was adopted to synthesize mesoporous, in-situ crystallized nitrogen doped TiO_2 in an amorphous Si-O-C-N matrix. The pyrolysis of pre-ceramic polymer in Ar/NH_3 atmosphere resulted in complete polymer to ceramic trans-formation leading to the formation of uniformly distributed nitrogen doped TiO_2 in an amorphous Si-O-C-N matrix. Pyrolysis in a reactive ammonia atmosphere has led to the inclusion of nitrogen atoms in the

TiO_2 lattice as well as in the amorphous matrix. The ammonia assisted pyrolysis treatment has also aided in the reduction of CMK-3 template, resulting in a high surface area (186 m^2/g) mesoporous nanocomposite. The mesoporous nanocomoposite exhibited high adsorption capacity and visible light photocatalytic activity towards degradation of me-thylene blue. The doping of nitrogen in to the TiO_2 lattice is expected to reduce the band gap, thereby harnessing light in the visible light wa-velength regime. The hydroxyl radicals and the superoxide anions formed are believed to degrade the organic molecules. The re-combination rate is expected to be lowered due to the formation of heterojunctions between the amorphous and crystalline phases.

References

[1] A. Fujishima, K. Honda, Electrochemical photolysis of water at a semiconductor electrode, Nature 238 (1972) 37–38.

[2] M. Anpo, M. Takeuchi, The design and development of highly reactive titanium oxide photocatalysts operating under visible light irradiation, J. Catal. 216 (2003) 505–516.

[3] J. Tang, J.R. Durrant, D.R. Klug, Mechanism of photocatalytic water splitting in TiO_2. Reaction of water with photoholes, importance of charge carrier dynamics, and evidence for four-hole chemistry, J. Am. Chem. Soc. 130 (2008) 13885–13891.

[4] S. Pavasupree, S. Ngamsinlapasathian, M. Nakajima, Y. Suzuki, S. Yoshikawa, Synthesis, characterization, photocatalytic activity and dye-sensitized solar cell performance of nanorods/nanoparticles TiO_2 with mesoporous structure, J. Photochem. Photobiol. A Chem. 184 (2006) 163–169.

[5] A. Houas, H. Lachheb, M. Ksibi, E. Elaloui, C. Guillard, J.-M. Herrmann, Photocatalytic degradation pathway of methylene blue in water, Appl. Catal. B Environ. 31 (2001) 145–157.

[6] J. Zhang, P. Zhou, J. Liu, J. Yu, New understanding of the difference of photo-catalytic activity among anatase, rutile and brookite TiO_2, Phys. Chem. Chem. Phys. 16 (2014) 20382–20386.

[7] N. Luo, Z. Jiang, H. Shi, F. Cao, T. Xiao, P.P. Edwards, Photo-catalytic conversion of oxygenated hydrocarbons to hydrogen over heteroatom-doped TiO_2 catalysts, Int. J. Hydrogen Energy. 34 (2009) 125–129.

[8] J.H. Xu, J. Li, W.L. Dai, Y. Cao, H. Li, K. Fan, Simple fabrication of twist-like helix N, S-codoped titania photocatalyst with visible-light response, Appl. Catal. B Environ. 79 (2008) 72–80.

[9] J.C. Yu, J. Yu, W. Ho, Z. Jiang, L. Zhang, Effects of F- doping on the photocatalytic activity and microstructures of nanocrystalline TiO_2 powders, Chem. Mater. 14 (2002) 3808–3816.

[10] X. Chen, C. Burda, The electronic origin of the visible-light absorption properties of C-, N- and S-doped TiO_2 nanomaterials, J. Am. Chem. Soc. 130 (2008) 5018–5019.

[11] R. Asahi, T. Morikawa, T. Ohwaki, K. Aoki, Y. Taga, Visible-light photocatalysis in nitrogen-doped titanium oxides, Science 293 (2001) 269–271.

[12] Q. Li, Y.W. Li, P. Wu, R. Xie, J.K. Shang, Palladium oxide nanoparticles on nitrogen-doped titanium oxide: accelerated photocatalytic disinfection and post-illumination catalytic "memory", Adv. Mater. 20 (2008) 3717–3723.

[13] S. Yin, Y. Aita, M. Komatsu, J. Wang, Q. Tang, T. Sato, Synthesis of excellent visible-light responsive $TiO_{2-x}N_y$ photocatalyst by a homogeneous precipitation-sol-vothermal process, J. Mater. Chem. 15 (2005) 674–682.

[14] S. Yin, Y. Aita, M. Komatsu, T. Sato, Visible-light-induced photocatalytic activity of $TiO_{2-x}N_y$ prepared by solvothermal process in urea–alcohol system, J. Eur. Ceram. Soc. 26 (2006) 2735–2742.

[15] S. Yin, K. Ihara, Y. Aita, M. Komatsu, T. Sato, Visible-light induced photocatalytic activity of $TiO_{2-x}A_y$ (A = N, S) prepared by precipitation route, J. Photochem. Photobiol. A Chem. 179 (2006) 105–114.

[16] H.-H. Tseng, W.W. Lee, M.-C. Wei, B.-S. Huang, M.-C. Hsieh, P.-Y. Cheng, Synthesis of TiO_2/SBA-15 photocatalyst for the azo dye decolorization through the polyol method, Chem. Eng. J. 210 (2012) 529–538.

[17] E. Ionescu, H.-J. Kleebe, R. Riedel, H. Xu, J.A.P. Cha, P.C.L. Wong, G. Wen, X. Zhang, X. Jing, F. Wang, B.Z. Tang, U.A. Jayasooriya, D. Hourlier, H.-J. Kleebe, G.D. Soraru, S. Enzo, F. Babonneau, Silicon-containing polymer-derived ceramic nanocomposites (PDC-NCs): preparative approaches and properties, Chem. Soc. Rev. 41 (2012) 5032.

[18] M. Zaheer, T. Schmalz, G. Motz, R. Kempe, Polymer derived non-oxide ceramics modified with late transition metals, Chem. Soc. Rev. Chem. Soc. Rev. 41 (2012) 5102–5116.

[19] S. Bernard, P. Miele, Ordered mesoporous polymer-derived ceramics and their processing into hierarchically porous boron nitride and silicoboron carbonitride monoliths, New J. Chem. 38 (2014) 1923.

[20] E. Ionescu, H.J. Kleebe, R. Riedel, Silicon-containing polymer-derived ceramic nanocomposites (PDC-NCs): Preparative approaches and properties, Chem. Soc. Rev. 41 (2012) 5032–5052.

[21] P. Colombo, G. Mera, R. Riedel, G.D. Sorarù, Polymer-derived ceramics: 40 years of research and innovation in advanced ceramics, J. Am. Ceram. Soc. 93 (2010) 1805–1837.

[22] R. Riedel, G. Mera, R. Hauser, A. Klonczynski, Silicon-based polymer-derived ceramics: synthesis properties and applications-a review dedicated to Prof. Dr. Fritz Aldinger on the occasion of his 65th birthday, J. Ceram. Soc. Jpn. 114 (1330) (2006) 425–444.

[23] L. Meng, X. Zhang, Y. Tang, K. Su, J. Kong, Hierarchically porous silicon-carbon-nitrogen hybrid materials towards highly efficient and selective adsorption of or-ganic dyes, Sci. Rep. 5 (2015) 7910.

[24] Y. Shi, Y. Wan, Y. Zhai, R. Liu, Y. Meng, B. Tu, D. Zhao, Ordered mesoporous SiOC and SiCN ceramics from atmosphere-assisted in situ transformation, Chem. Mater. 19 (2007) 1761–1771.

[25] H. Bréquel, J. Parmentier, S. Walter, R. Badheka, G. Trimmel, S. Masse, J. Latournerie, P. Dempsey, C. Turquat, A. Desmartin-Chomel, L. Le Neindre-Prum, U.A. Jayasooriya, D. Hourlier, H.J. Kleebe, G.D. Sorarù, S. Enzo, F. Babonneau, Systematic structural characterization of the high-temperature behavior of nearly stoichiometric silicon oxycarbide glasses, Chem. Mater. 16 (2004) 2585–2598.

[26] H. Fukui, K. Eguchi, H. Ohsuka, T. Hino, K. Kanamura, Structures and lithium storage performance of Si-O-C composite materials depending on pyrolysis tem-peratures, J. Power Sources 243 (2013) 152–158.

[27] N. Subramanian, B. Viswanathan, Nitrogen- and oxygen-containing activated car-bons from sucrose for electrochemical supercapacitor applications, RSC Adv. 5 (2015) 63000–63011.

[28] M.C. Bechelany, V. Proust, A. Lale, P. Miele, S. Malo, C. Gervais, S. Bernard, Nanocomposites through the chemistry of single-source precursors: understanding the role of chemistry behind the design of monolith-type nanostructured titanium nitride/silicon nitride, Chem. – Eur. J. 23 (2017) 832–845.

[29] M.C. Bechelany, V. Proust, C. Gervais, R. Ghisleni, S. Bernard, P. Miele, In situ controlled growth of titanium nitride in amorphous silicon nitride: a general route toward bulk nitride nanocomposites with very high hardness, Adv. Mater. 26 (2014) 6548–6553.

[30] C. Di Valentin, E. Finazzi, G. Pacchioni, A. Selloni, S. Livraghi, M.C. Paganini, E. Giamello, N-doped TiO_2: theory and experiment, Chem. Phys. 339 (2007) 44–56.

[31] D. Kusano, M. Emori, H. Sakama, Influence of electronic structure on visible light photocatalytic activity of nitrogen-doped TiO_2, RSC Adv. 7 (2017) 1887–1898.

[32] H. Chen, A. Nambu, W. Wen, J. Graciani, Z. Zhong, J.C. Hanson, E. Fujita, J.A. Rodriguez, Reaction of NH_3 with titania: N-doping of the oxide and TiN for-mation, J. Phys. Chem. C 111 (2007) 1366–1372.

[33] M.A. Abass, A.A. Syed, C. Gervais, G. Singh, Synthesis and electrochemical per-formance of a polymer-derived silicon oxycarbide/boron nitride nanotube compo-site, RSC Adv. 7 (2017) 21576–21584.

[34] L. Yan, G. Chen, S. Tan, M. Zhou, G. Zou, S. Deng, S. Smirnov, H. Luo, Titanium oxynitride nanoparticles anchored on carbon nanotubes as energy storage mate-rials, ACS Appl. Mater. Interfaces 7 (2015) 24212–24217.

[35] D.-H. Wang, L. Jia, X.-L. Wu, L.-Q. Lu, A.-W. Xu, One-step hydrothermal synthesis of N-doped TiO_2/C nanocomposites with high visible light photocatalytic activity, Nanoscale 4 (2012) 576–584.

[36] W. Wang, Y. Liu, J. Qu, Y. Chen, Z. Shao, Nitrogen-doped TiO_2 microspheres with hierarchical micro/nanostructures and rich dual-phase junctions for enhanced photocatalytic activity, RSC Adv. 6 (2016) 40923–40931.

[37] R. Wang, Q. Wu, Y. Lu, H. Liu, Y. Xia, J. Liu, D. Yang, Z. Huo, X. Yao, Preparation of nitrogen-doped TiO_2/graphene nanohybrids and application as counter electrode for dye-sensitized solar cells, ACS Appl. Mater. Interfaces. 6 (2014) 2118–2124.

[38] S. Kohn, W. Hoffbauer, M. Jansen, R. Franke, S. Bender, Evidence for the formation of SiON glasses, J. Non. Cryst. Solids 224 (1998) 232–243.

[39] F. Hayashi, K.I. Ishizu, M. Iwamoto, Fast and almost complete nitridation of me-soporous silica MCM-41 with ammonia in a plug-flow reactor, J. Am. Ceram. Soc. 93 (2010) 104–110.

[40] R. Kalfat, F. Babonneau, N. Gharbi, H. Zarrouk, 29Si MAS NMR investigation of the pyrolysis process of cross-linked polysiloxanes prepared from poly-methylhydrosiloxane, J. Mater. Chem. 6 (1996) 1673–1678.

[41] Y. Ao, J. Xu, D. Fu, C. Yuan, A simple route for the preparation of anatase titania-coated magnetic porous carbons with enhanced photocatalytic activity, Carbon N. Y. 46 (2008) 596–603.

[42] S. Adachi, Optical Properties of Crystalline and Amorphous Semiconductors: Materials and Fundamental Principles, Kluwer Academic Publishers, Boston, 1999.